Available online at www.sciencedirect.com
SCIENCE DIRECT
Journal of Power Sources 157 (2006) 543–549
JOURNAL OF POWER SOURCES
www.elsevier.com/locate/jpowsour

Carbon structure/function relationships: Characterization and electrochemistry of carbon nanofibers

Kenneth J. Takeuchi [a,*], Amy C. Marschilok [a], Garret C. Lau [a], Randolph A. Leising [b], Esther S. Takeuchi [b]

[a] *Department of Chemistry, University at Buffalo (SUNY), Box 603000, Buffalo, NY 14260-3000, USA*
[b] *Greatbatch, Inc., 10,000 Wehrle Dr., Clarence, NY 14031, USA*

Received 17 May 2005; received in revised form 20 June 2005; accepted 20 June 2005
Available online 21 September 2005

Abstract

We report here the characterization and electrochemistry of a new type of carbon nanofiber that was prepared in our laboratories. In addition, two different commercially available carbons, carbon black (Shawinigan black AB50P) and synthetic graphite (LK702) are studied in parallel to benchmark the properties of our carbon nanofibers. Physical characterizations include X-ray diffraction, methylene blue adsorption, Brunauner–Emmett–Teller surface area analysis, and thermogravimetric analysis. Carbon electrochemistries are interrogated in coin-sized cells versus lithium electrodes. Correlations are noted, and explanations are offered to describe broader carbon structure/function relationships.

Keywords: Carbon nanofiber; Carbon black; Graphite; Electrochemistry; X-ray diffraction; Surface area

1. Introduction

Carbon nanofibers are a specific family of carbons formed from the interaction of finely divided metal catalyst particles with carbon containing gases at elevated temperatures [1]. Iron-based materials have been found to be some of the most active catalysts for carbon deposition, and therefore the use of various iron containing catalysts for carbon nanofiber formation has been investigated for a number of years [2–10]. By modifying the chemical composition [7] and morphology [22] of the catalyst used, the carbon nanofiber fine structure and gross morphology can be independently tuned. Additionally, by modifying the composition and flow rate of the carbonaceous feed gas, the gross diameter of the carbon nanofibers produced can be controlled [9]. These characteristics make carbon nanofibers highly attractive for fundamental studies of structure/function relationships. Carbon nanofiber fine structures range from tubular arrangements with graphitic planes oriented parallel to the major fiber axis, to edge-exposed, flat stacked platelets with graphitic planes oriented perpendicular to the major fiber axis [7,11]. Intermediate edge exposed structures also exist, in which the graphitic planes are at an acute angle with respect to the major fiber axis. Our carbon nanofibers fall within the intermediate edge category (Fig. 1) [22].

Previous electrochemical studies of carbon nanofibers have focused primarily on their use as electrode materials for cyclic voltammetry [12–15], with some studies focusing on carbon nanotubes specifically [10,16–19]. Recently, there has been some investigation of the use of carbon nanofiber electrodes for lithium-ion batteries [20,21].

A different approach to benchmark the physical and electrochemical characteristics of carbon nanofibers is presented here. The physical and electrochemical properties of the carbon nanofibers are compared to two inherently different carbons, carbon black (Shawinigan black AB50P) and synthetic graphite (LK702). Carbon black and synthetic graphite were chosen because they represent two extremes in the range of commercially available carbons: carbon blacks are disordered carbons, with higher BET surface areas, smaller crystallite sizes, and larger d_{002} spacings, while synthetic graphites are ordered carbons, with lower BET surface areas, larger crystallite sizes, and smaller d_{002} spacings. Characterizing our carbon nanofibers

* Corresponding author. Tel.: +1 716 645 2872; fax: +1 716 645 6963.
E-mail addresses: takeuchi@buffalo.edu (K.J. Takeuchi), acm@buffalo.edu (A.C. Marschilok), RLeising@greatbatch.com (R.A. Leising), ETakeuchi@greatbatch.com (E.S. Takeuchi).

0378-7753/$ – see front matter © 2005 Elsevier B.V. All rights reserved.
doi:10.1016/j.jpowsour.2005.06.036

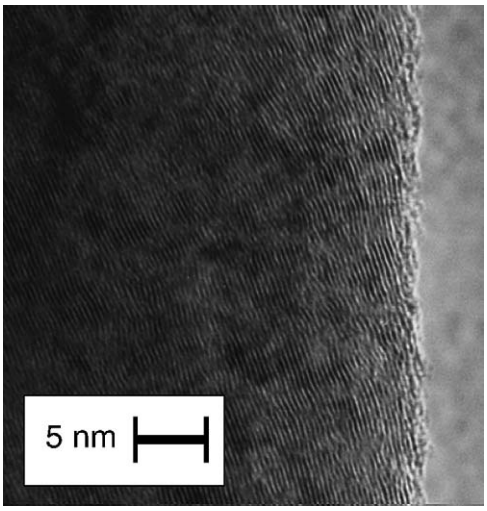

Fig. 1. Fine structure of carbon nanofibers from acicular and granular iron catalysts.

using the same criteria as commercially available carbons serves multiple purposes. First, it allows the properties of our carbon nanofibers to be benchmarked relative to more familiar materials. Additionally, identifying correlations among physical and electrochemical characteristics, which occur in several different types of carbon can help to understand broader carbon structure/function relationships. Electrochemistry is characterized using carbon-based electrodes versus lithium metal electrodes in coin-sized cells. X-ray diffraction, methylene blue adsorption, Brunauner–Emmett–Teller (BET) surface area analysis, and thermogravimetric analysis are also performed to interrogate the physical properties of the carbons studied.

2. Experimental

2.1. Carbon preparation

Via quantitative control of experimental variables, we were successful in preparing highly granular and highly acicular samples of finely divided iron from the hydrotriorganoborate reduction of iron(III) chloride [22]. We then utilized the granular and acicular iron samples as catalysts for the formation of two new types of carbon nanofibers with similar fine structures, but differing gross morphologies. High resolution transmission electron microscopy (HRTEM) showed carbon nanofibers formed from both acicular and granular iron catalysts to have graphitic planes oriented at an acute angle with respect to the major fiber axis (Fig. 1).

Carbon nanofibers formed from granular iron catalysts predominately showed a spiral gross morphology, while carbon nanofibers formed from acicular iron catalysts showed a straight gross morphology. Subsequent to synthesis, our carbon nanofibers were stirred in 1 M $HCl_{(aq)}$ for approximately 100 h to remove any residual iron, rinsed thoroughly with deionized water, then heated at 65 °C under vacuum for at least 36 h until constant mass was observed.

Synthetic graphite (LK702) was purchased from Nippon Carbon Company. Carbon black (Shawinigan AB 50P) was purchased from Chevron. Prior to characterization and use in electrode preparation, synthetic graphite and carbon black were each heated at 65 °C under vacuum for at least 36 h, similar to the carbon nanofiber treatment.

2.2. Physical characterization

Carbon samples were characterized using X-ray diffraction (XRD), thermogravimetric analysis (TGA), differential thermal analysis (DTA), Brunauner–Emmett–Teller surface area, and methylene blue (3,7-bis(dimethylamino)phenothiazin-5-ium chloride) adsorption techniques (Table 1). XRD data were collected with a Shimadzu Lab X-6000 X-ray diffractometer using fixed divergence and scatter slits of 1.00 mm, a receiving slit of 0.30 mm, and Cu Kα radiation. The samples were contained in an aluminum well holder with a sample chamber 25 mm in diameter and 1 mm deep. The spacing between adjacent carbon layers (d_{002}) was determined using the Bragg equation, while the dimensions of crystallites with graphite-like order (L_{002} and L_{100}) were calculated using the Scherrer equation ($L = K\lambda/B\cos\vartheta$) and the values of the (0 0 2) and (1 0 0) reflections, respectively. For the 0 0 2 reflection, $K = 0.89$, while for the

Table 1
Physical characterizations

Carbon type	Surface area			Mass lost[b] (%)	Crystallite parameters				
	BET ($m^2\ g^{-1}$)	Methylene blue ($m^2\ g^{-1}$)	A[a] (%)		d_{002} (Å)	L_{002} (Å)	L_{100} (Å)	L_{002}/L_{100}	$((L_{002}/d_{002})+1)^{-1}$
Graphite	3	1	33	4	3.38	201	455	0.44	0.017
Carbon black	65	12	18	17	3.53	50	–[d]	–	0.066
Carbon nanofibers (from acicular Fe)	214	–[c]	–	100	3.40	63	101	0.62	0.051
Carbon nanofibers (from granular Fe)	178	8	5	93	3.41	79	144	0.55	0.041

[a] A, or accessible area, is the percentage of methylene blue surface area relative to BET surface area.[29].
[b] Mass lost is percent mass lost during CO_2 treatment at 1100 °C.
[c] The methylene blue surface area for carbon nanofibers (from acicular Fe) was not measured.
[d] The 1 0 0 peak for carbon black was too low in intensity to be accurately measured.

1 0 0 reflection, $K = 1.84$ was used [23]. While other authors have used the (1 1 0) reflection to estimate the length of the carbon crystallite basal plane (L_a) [31], the (1 0 0) reflection was used in this case because the overlap between the graphite(1 1 0) peak and the (3 1 1) peak of the aluminum sample holder made deconvolution of the graphite(1 1 0) peak difficult. Thermogravimetric (TG) analysis was performed using a TA Instruments SDT 2960 Simultaneous TGA-DTA. Carbon samples were outgassed for 15 min, then ramped to 1200 °C at a rate of 20° min^{-1}, under a $CO_{2(g)}$ flow of approximately 100 mL min^{-1}. A Micromeritics Gemini 5 automatic volume sorption analyzer was used for BET surface area analysis, using N_2 as an adsorbate at −196 °C. Carbon samples were flow outgassed under $N_{2(g)}$ at 120 °C for at least 1 h prior to BET analysis. Methylene blue and Triton-X reagents were purchased from Fisher Scientific. Five to 40 mg samples of carbon were stirred in 10 mL of a 20 μM aqueous methylene blue solution containing 0.2% Triton-X by volume for at least 20 h. The resulting solutions were then passed through 0.2 μm PTFE syringe filters (Gelman) into glass cuvettes. A Milton Roy Spectronic 1001 plus was used for methylene blue adsorption measurements, with absorbance measurements made at λ = 661.0 nm. Using a value of 170 A^2 per molecule of methylene blue, the surface area of the carbon was determined by monitoring the change in absorbance of the methylene blue solution after stirring in carbon [27].

2.3. Electrode preparation

A dry room with less than 0.5% humidity was used for all phases of electrode preparation. Unless otherwise noted, reagents used in electrode preparation were purchased from Aldrich Chemical Company. Using the four types of carbons discussed above, mixtures containing 91% carbon, 8% poly(vinylidene difluoride) (PVDF) (Kynar 461), and 1% oxalic acid by mass were suspended in sufficient dimethylformamide (DMF) or *n*-methyl pyrrolidinone (NMP) solvent to achieve slurries of desired consistency. The oxalic acid was used to etch the copper foil and improve adhesion of the carbon coating. The slurries were mixed at 450 rpm for 5–10 min using an overhead mixer, then spread onto a 0.023 mm thick sheet of electrodeposited Cu foil. A doctor blade handcoater was used for spreading the slurry, with the blade set to a height of 0.027–0.120 mm over the foil, depending on the carbon sample used (see Table 2 for details).

The resulting film was dried under vacuum at 100–110 °C for at least 12 h and pressed between two stainless steel plates at approximately 14 t cm^{-2} for 10 s. The thickness of the resulting carbon film was measured, and 16 mm diameter disks of the coated foil were punched out for use as coin cell electrodes. Each electrode used contained 6–10 mg of carbon.

2.4. Coin cell preparation

A dry room with less than 1% relative humidity was used for all phases of coin cell preparation. Coin-sized sample cells were made using the coated copper foil electrodes versus metallic lithium electrodes, a method widely used for analysis of carbons in lithium-ion batteries [24,25]. The metallic lithium electrodes used were 18 mm in diameter with masses of 50 mg. An electrolyte solution of 1 M lithium hexafluorophosphate in a 30:70% (v/v) ethylene carbonate (EC):dimethylcarbonate (DMC) mixture (EM industries Selectipur®) was used. A microporous polyethylene film was used to separate the two electrodes, a polypropylene gasket was used to electrically isolate the two sides of the stainless steel case, and nickel leads were used to make electrical contact with each side of the case. A stainless steel spring and spacer were used to fill the excess coin cell case volume.

2.5. Electrochemical characterization

Electrochemical characterization was performed using a Bitrode SCN 48-0.5/0.05-5BP Cycle Life Tester. The general procedure used was as follows: (1) the cells were charged under a constant current (lithium was inserted into the carbon electrode) until a terminal voltage was achieved; (2) the cells were then charged at constant voltage until the current dropped below a specified level; (3) after resting the cells at open circuit potential, discharge (lithium deintercalation from the carbon electrode) was allowed to occur at constant current to a set voltage; (4) the cells were then rested at open circuit potential. The cells were subjected to several charge/discharge cycles with data collected continuously. Limiting conditions for the intercalation and deintercalation steps were selected to optimize test efficiency versus test equipment capability. The capacity of each cell was determined from the maximum deintercalation capacity during the capacity/stability test (Table 3), to provide a measure of the usable capacities of the different types of carbon under similar test conditions. The *C* rate for each cycle was determined from the current at that cycle divided by the cell capacity. Average gravimetric capacities for each type of carbon were then determined. The results reported are average val-

Table 2
Electrode coating parameters

Carbon type	Blade height (mm)	Current density[a] (mA cm^{-2})	Coating thickness after press (mm)
Graphite	0.09	1.11	0.03
Carbon black	0.50	0.75	0.12
Carbon nanofibers (from acicular Fe)	0.25	0.75	0.07
Carbon nanofibers (from granular Fe)	0.25	1.12	0.07

[a] Deintercalation current for cycles 6–55, 61–120/area of carbon electrode.

Table 3
Electrochemical test parameters

Test phase	Cycles	Intercalation I[a]	Intercalation II	Deintercalation[a]
Formation	1–5	*C*/2 to 0.011 V	0.011 V to <*C*/4	*C*/2 to 1.50 V
Capacity/stability	6–55	1.2*C* to 0.011 V	0.011 V to <*C*/4	1.2*C* to 1.25 V
Discharge capacity	56	1.0*C* to 0.011 V	0.011 V to <*C*/5	*C*/5 to 1.25 V

[a] Each intercalation I and deintercalation was preceded by a 30 min rest at open circuit potential.

ues from at least two coin-sized cells for each type of carbon studied.

3. Results and discussion

3.1. Physical properties

After measuring the physical properties of all of the different carbons (Table 1), a series of linear regression analyses was performed to determine how they interrelate. Interestingly, the data for BET surface area and methylene blue surface area did not correlate well. Methylene blue has been previously established to be a useful adsorptive for surface area analysis of solids [26–29]. A comparison of methylene blue surface area and BET surface area can be used to estimate porosity, as methylene blue is a much larger molecule which cannot access the smaller pores which $N_{2(g)}$ can access [27]. Assuming that the carbons of interest do not have significant hydrocarbon functionalities, the quantity of methylene blue adsorbed can be a measure of the surface of the carbon, which is accessible by larger molecules, including pores greater than 1.3 nm in diameter [29]. The ratio of the methylene blue surface area to the BET surface area is described as methylene blue accessibility, *A*, in Table 1.

A linear positive correlation was observed between BET surface area and percent mass lost by TG analysis in $CO_{2(g)}$ (Fig. 2a). This correlation was more linear than those between percent mass lost and methylene blue surface area and between percent mass lost and accessible area ratios, suggesting that much of the surface area measurable by BET ($N_{2(g)}$ adsorbate) is available for reaction with $CO_{2(g)}$. Interestingly, for the three carbons in which L_{100} could be measured, the correlation between L_{100} and percent mass lost was excellent (Fig. 2b), suggesting that mass lost in $CO_{2(g)}$ may be influenced by the crystallite dimensions as well as by gross particle characteristics like BET surface area.

Notably, for the three carbons in which L_{100} and L_{002} were both determined a linear positive correlation was evident (Fig. 2c). This shows that for this group of carbons, the synthetic graphite had the largest crystallites in both the L_a and L_c dimensions, while the carbon nanofibers made from acicular iron had the smallest crystallites in both dimensions.

3.2. Electrochemistries

Coin-sized cells were subjected to 56 charge/discharge cycles, predominantly at a 1.2*C* rate (see Table 3 above for details). This high *C* rate was selected to provide a basis for comparison of the electrochemistries of the carbons under fast charge/discharge conditions. After the first five formation cycles, synthetic graphite showed a steady decrease in deintercalation capacity with increasing cycle number (Fig. 3). Similarly, carbon black showed a gradual decrease in deintercalation capacity after the first 10 cycles. In contrast, both forms of carbon nanofibers showed a distinctive increase in both intercalation and deintercalation capacity over the first 20 cycles. Thus, discharge capacities were determined at a *C*/5.1 rate during cycle 56, after the carbon nanofibers had reached their maximal capacity (Table 4). Although the different carbons showed different capacity versus cycle number trends, the cycle 56 measurement was selected to

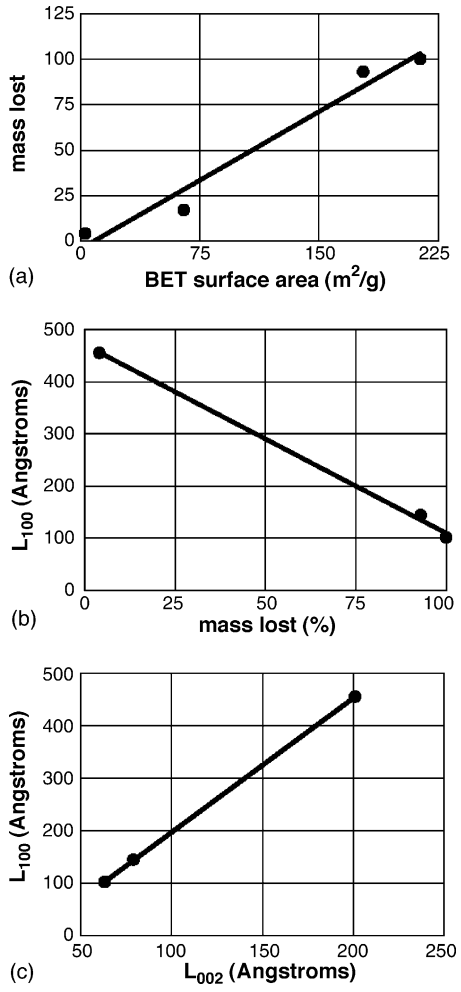

Fig. 2. Correlation of physical characterization parameters: (a) mass lost and BET surface area, (b) L_{100} and mass lost, and (c) L_{100} and L_{002}.

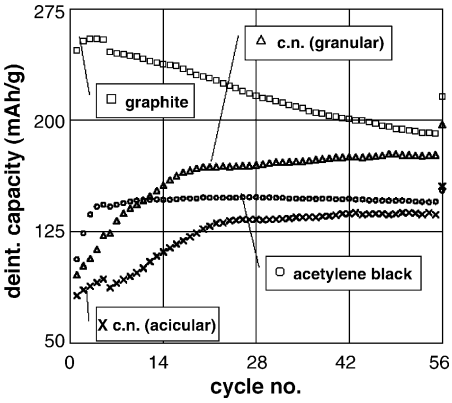

Fig. 3. Deintercalation capacities of carbons in coin-sized cells vs. lithium metal electrodes.

provide a snapshot of the discharge capacities of the different carbons at the same test time.

Analysis of the charge/discharge data showed carbon nanofibers to function effectively as electrode materials, although with low capacity (Table 4). The carbon nanofibers formed from granular iron catalysts showed a slightly higher discharge capacity than those formed from acicular iron catalysts, suggesting that the gross morphologies of the carbon nanofibers can have some impact on their electrochemistries in lithium-ion cells.

Winter et al. noted a positive linear correlation between irreversible capacity and surface area in some Timrex graphites [30]. Additionally, they noted that the ratio of basal to prismatic (edge) surface area and the particle size distribution are important considerations which can overwhelm the effects of BET surface area on irreversible capacity when comparing different types of carbon. Although the L_{002}/L_{100} ratios differed significantly for the carbons in this study (Table 1), a linear positive correlation between BET surface area and irreversible capacity was still evident (Fig. 4a). It is interesting to note that while there was not a good linear correlation between methylene blue surface area and irreversible capacity, there was a linear negative correlation between methylene blue accessibility (value *A*, Table 1) and irreversible capacity (Fig. 4b). Thus, as the *fraction* of the BET surface area that was accessible to methylene blue decreases, the irreversible capacity increases. Also, there was a linear negative correlation between methylene blue surface area and discharge capacity (Fig. 4c). These two observations are consistent with methylene blue adsorption occurring primarily on the exposed planar graphitic surfaces and not within the layers or on the edges of the carbons.

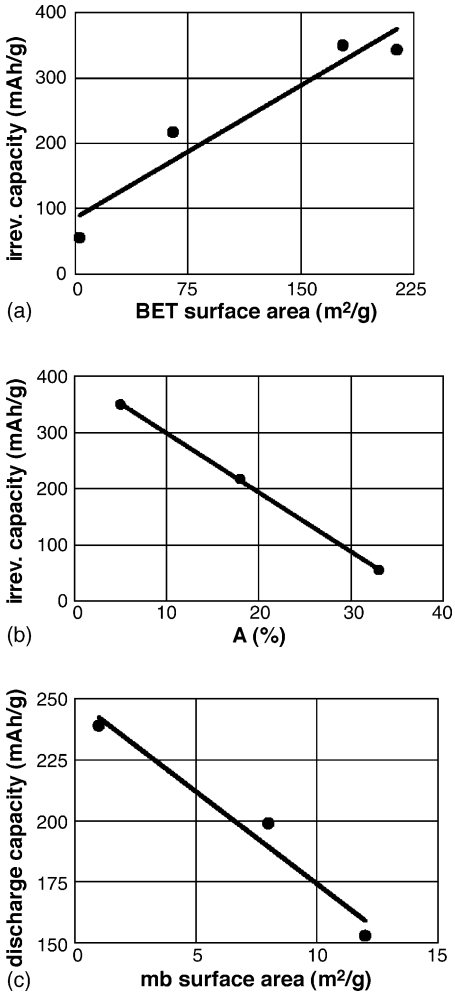

Fig. 4. Correlation of capacities and surface area: (a) irreversible capacity and BET surface area, (b) irreversible capacity and methylene blue accessibility (*A*), and (c) discharge capacity and methylene blue (mb) surface area.

Table 4
Electrochemical test results

Carbon type	Discharge capacity[b] (mAh g^{-1})[a]	Irreversible capacity[c] (mAh g^{-1})[a]
Graphite	239	55
Carbon black	153	217
Carbon nanofibers (from acicular Fe)	156	343
Carbon nanofibers (from granular Fe)	199	350

[a] Grams used in calculations were masses of carbon only.
[b] Discharge capacity is deintercalation capacity at *C*/5.1 rate (cycle 56).
[c] Irreversible capacity is cycle 1 intercalation capacity–cycle 1 deintercalation capacity.

Recently, "active surface area" was discussed by Kinoshita and coworkers, where edge sites were proposed to be catalytically more active toward electrolyte decomposition than basal sites, and thus, the greater the active surface area of a carbon, the greater its irreversible capacity [31]. Assuming nonporous prismatic carbon crystallites oriented regularly with respect to one another, as the basal dimension L_a increases the proportion of active surface area decreases, and as the edge dimension L_c increases the active surface area increases. Irreversible capacity was therefore predicted to increase linearly as a function of $1/L_a$. The results for our study were consistent with this active surface area definition, as a linear increase in irreversible capacity occurred as a function of $1/L_{100}$ (Fig. 5a).

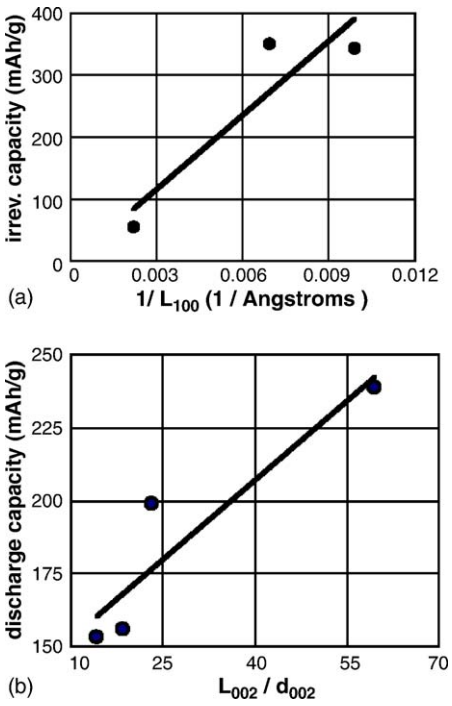

Fig. 5. Correlation of capacity and crystallite parameters: (a) irreversible capacity and $1/L_{100}$ and (b) discharge capacity and number of graphitic layers (L_{002}/d_{002}).

In their studies of disordered carbons in lithium-ion batteries, Wang and coworkers described three different locations for lithium–carbon interaction: edge sites, in which lithium species were located on the edges of graphitic layers; surface sites (or basal) sites, in which lithium species were located on the basal plane surfaces of the crystallites, and layer sites, in which the lithium species were intercalated between graphitic layers [32]. The number of layers in a crystallite was then determined using L_c/d_{002}. For disordered carbons with a large L_c and an $L_a < 100$ Å, the discharge capacity was found to increase as the number of layers decreased. For the carbons of our study, the discharge capacity increased as the number of layers increased (Fig. 5b). For the disordered (small L_a) carbons in the study by Wang and coworkers, increasing graphitic layers generated a larger area of unstable edge sites, but a relatively small area of stable basal sites. Therefore, the deleterious edge effects dominated, and the discharge capacity decreased with increasing graphitic layers. In contrast, for the carbons of our study, increasing graphitic layers generated a more significant area of stable basal sites, resulting in a net increase in discharge capacity with increasing graphitic layers.

4. Conclusions

The characterization and electrochemistry of new carbon nanofibers were conducted and compared to two different commercially available carbons, carbon black (Shawinigan black AB50P) and synthetic graphite (LK702). Correlations among physical properties and electrochemical results were conducted to probe structure/function relationships associated with carbon electrochemistry. Some of the notable observations were: a linear negative correlation between methylene blue accessibility and irreversible capacity; a linear positive correlation between $1/L_{100}$ and irreversible capacity; a linear positive correlation between L_{002}/d_{002} and discharge capacity. In addition, the gross morphologies of the carbon nanofibers appeared to have some impact on their electrochemistries in lithium-ion cells, as carbon nanofibers with similar carbon edge orientations and d_{002} spacings but different gross morphologies had different discharge capacities.

Acknowledgement

This work was supported in part by a grant from the Research Corporation (ROA).

References

[1] K.P. De Jong, J.W. Geus, Catal. Rev. Sci. Eng. 42 (2000) 481.
[2] R.T.K. Baker, J.R. Alonzo, J.A. Dumesic, D.J.C. Yates, J. Catal. 77 (1982) 74.
[3] R.T.K. Baker, J.J. Chludzinski Jr., C.R.F. Lund, Carbon 25 (1997) 295.
[4] R.T.K. Baker, N.M. Rodriguez, Novel Forms of Carbon II, Materials Research Society, Pittsburgh, 1994.
[5] N. Krishnankutty, N.M. Rodriguez, R.T.K. Baker, J. Catal. 158 (1996) 217.
[6] C. Park, N.M. Rodriguez, R.T.K. Baker, J. Catal. 169 (1997) 212.
[7] N.M. Rodriguez, A. Chambers, R.T.K. Baker, Langmuir 11 (1995) 3862.
[8] P.E. Anderson, N.M. Rodriguez, Chem. Mater. 12 (2000) 823.
[9] Y.Y. Fan, H.M. Cheng, Y.L. Wei, G. Su, Z.H. Shen, Carbon 38 (2000) 921.
[10] G.T. Wu, C.S. Wang, X.B. Zhang, H.S. Yang, Z.F. Qi, P.M. He, W.Z. Li, J. Electrochem. Soc. 146 (1999) 1696.
[11] C. Park, P.E. Anderson, A. Chambers, C.D. Tan, R. Hidalgo, N.M. Rodriguez, J. Phys. Chem. B 103 (1999) 10572.
[12] N. van Dijk, S. Fletcher, C.E. Madden, F. Marken, Analyst 126 (2001) 1878.
[13] F. Marken, M.L. Gerrard, I.M. Mellor, R.J. Mortimer, C.E. Madden, S. Fletches, K. Holt, J.S. Foord, R.H. Dahm, F. Page, Electrochem. Commun. 3 (2001) 177.
[14] S. Maldonado, K.J. Stevenson, J. Phys. Chem. B 31 (2004) 11375.
[15] M.A. Guillorn, T.E. McKnight, A. Melechko, V.I. Merkulov, P.F. Britt, D.W. Austin, D.H. Lowndes, M.L. Simpson, J. Appl. Phys. 91 (2002) 3824.
[16] Y.P. Wu, E. Rahm, R. Holze, J. Power Sources 114 (2003) 228.
[17] F. Leroux, K. Méténier, K.S. Gautier, E. Frackowiak, S. Bonnamy, F. Béguin, J. Power Sources 81–82 (1999) 317.
[18] D. Aurbach, J.S. Gnanaraj, M.D. Levi, E.A. Levi, J.E. Fischer, A. Claye, J. Power Sources 97–98 (2001) 92.
[19] E. Frackowiak, F. Béguin, Carbon 140 (2002) 775.
[20] T. Doi, A. Fukuda, Y. Iriyama, T. Abe, Z. Ogumi, K. Nakagawa, T. Ando, Electrochem. Commun. 7 (2005) 10.
[21] S.H. Yoon, C.W. Park, H. Yang, Y. Korai, I. Mochida, R.T.K. Baker, N.M. Rodriguez, Carbon 42 (2004) 21.
[22] K.J. Takeuchi, A.C. Marschilok, C.A. Bessel, N.R. Dollahon, J. Catal. 208 (2002) 150.
[23] K. Kinoshita, Carbon: Electrochemical and Physicochemical Properties, John Wiley and Sons Inc., New York, 1988.
[24] T. Zheng, Y. Liu, E.W. Fuller, S. Tsend, U. von Sacken, J.R. Dahn, J. Electrochem. Soc. 142 (1995) 2581.
[25] J.R. Dahn, A.K. Sleight, H. She, J.N. Reimers, Q. Zhong, B.M. Way, Electrochim. Acta 38 (1993) 1179.

[26] C. Kaewprasit, E. Hequet, N. Abidi, J.P. Courlot, J. Cotton Sci. 2 (1998) 164.
[27] R.S. Rubino, E.S. Takeuchi, J. Power Sources 81–82 (1999) 373.
[28] S.S. Barton, Carbon 25 (1987) 343.
[29] D. Graham, J. Phys. Chem. 59 (1955) 896.
[30] M. Winter, P. Novák, A. Monnier, J. Electrochem. Soc. 145 (1998) 428.
[31] T. Tran, B. Yebka, X. Song, G. Nazri, K. Kinoshita, D. Curtis, J. Power Sources 85 (2000) 269.
[32] Y. Matsumura, S. Wang, J. Mondori, Carbon 33 (1995) 1457.